

Supplementary Materials for

Nanoporous hydrogen-bonded organic framework for high performance photocatalysis

Xiuyan Cheng,^{a,b} Jianling Zhang,^{*a,b} Yufei Sha,^{a,b} Mingzhao Xu,^{a,b} Ran Duan,^c Zhuizhui Su,^{a,b} Jiali Li,^d Yanyue Wang,^{a,b} Jingyang Hu,^{a,b} Bo Guan,^e and Buxing Han^{a,b}

^aBeijing National Laboratory for Molecular Sciences, CAS Key Laboratory of Colloid, Interface and Chemical Thermodynamics, CAS Research/Education Center for Excellence in Molecular Sciences, Institute of Chemistry, Chinese Academy of Sciences, Beijing 100190, P.R.China.

^bSchool of Chemical Sciences, University of Chinese Academy of Sciences, Beijing 100049, P.R.China.

^cKey Laboratory of Photochemistry, Institute of Chemistry, Chinese Academy of Sciences, Beijing 100190, P.R.China.

^dCenter for Physicochemical Analysis and Measurement, Institute of Chemistry, Chinese Academy of Sciences Beijing 100190, P. R. China

^eBeijing Synchrotron Radiation Facility (BSRF), Institute of High Energy Physics, Chinese Academy of Sciences, Beijing 100049, P.R.China.

*Correspondence to: zhangjl@iccas.ac.cn

Results and Discussion

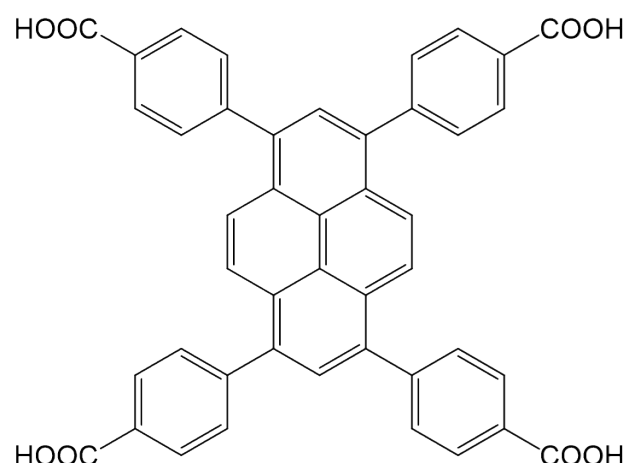


Fig. S1. Molecular structure of H₄TBAPy.

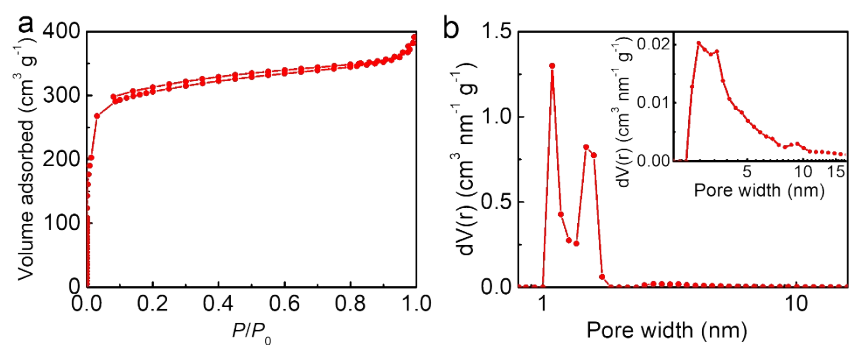


Fig. S2. N₂ adsorption-desorption isotherm (a) and pore size distribution curve (b) of *p*-PFC-1.

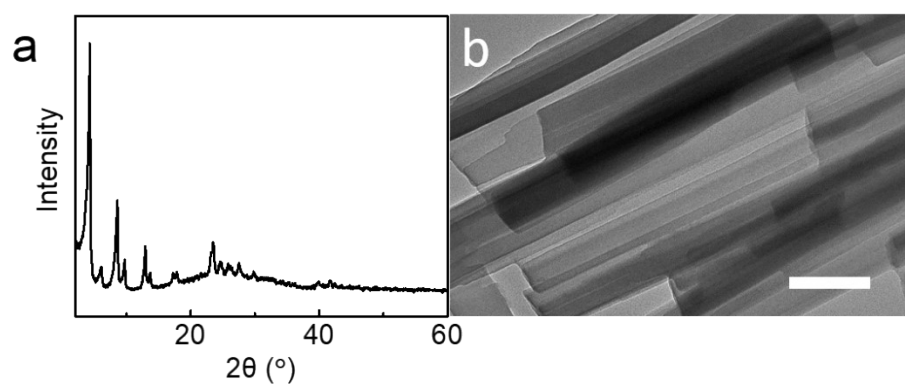


Fig. S3. XRD pattern (a) and TEM image (b) of o-PFC-1. Scale bar: 200 nm in (b).

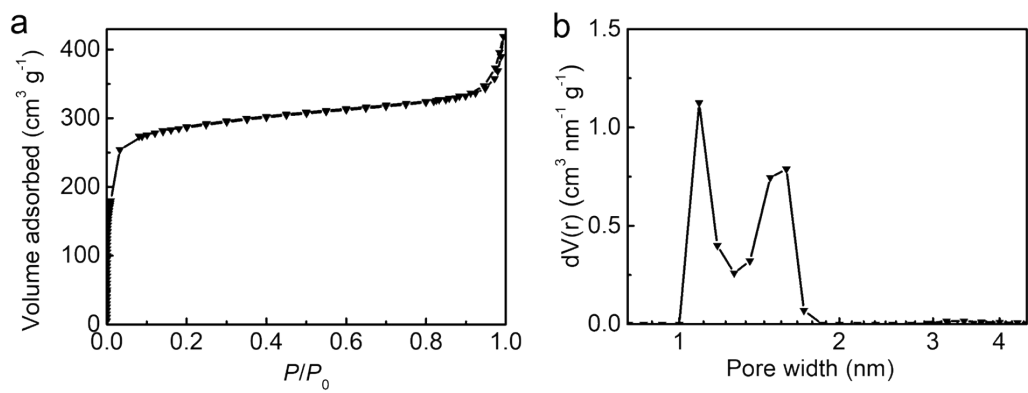


Fig. S4. (a) N₂ adsorption-desorption isotherm and (b) pore size distribution curve of o-PFC-1.

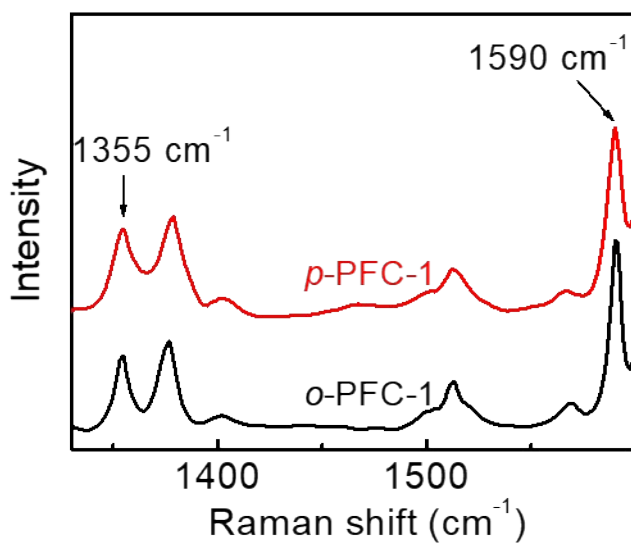


Fig. S5. Raman spectra of *p*-PFC-1 and *o*-PFC-1.

Raman spectrum of *p*-PFC-1 exhibits characteristic D and G bands at 1355 and 1591 cm^{-1} , respectively, which is similar to those of graphene nanoribbons.¹ The D band is attributed to the disorder in the carbon materials, while the G band signifies graphitizing feature caused by sp^2 networks. Accordingly, the intensity ratio of D-band to G-band (I_D/I_G) is indicative of disorder degree. For *p*-PFC-1, I_D/I_G is estimated to be 0.46, which is higher than that of *o*-PFC-1 (0.39), implying higher degree of disorder in *p*-PFC-1.²

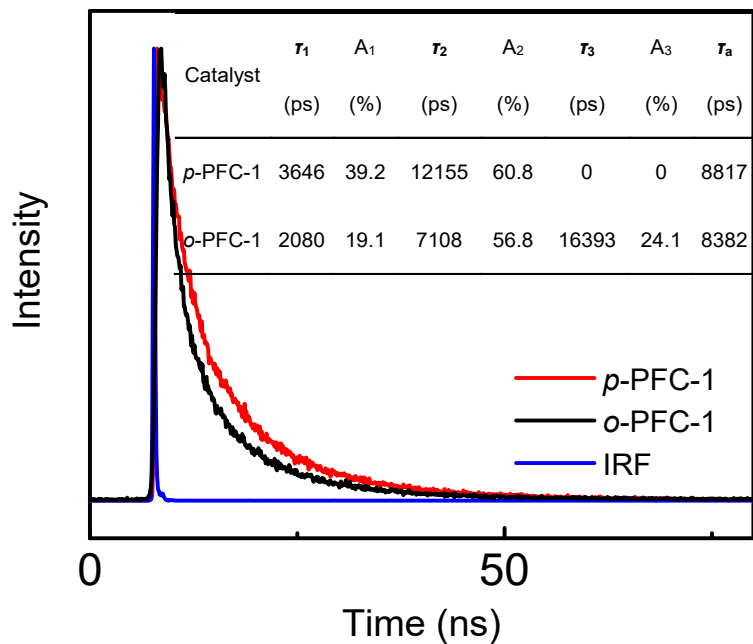


Fig. S6. TRFDS spectra of *p*-PFC-1 and *o*-PFC-1.

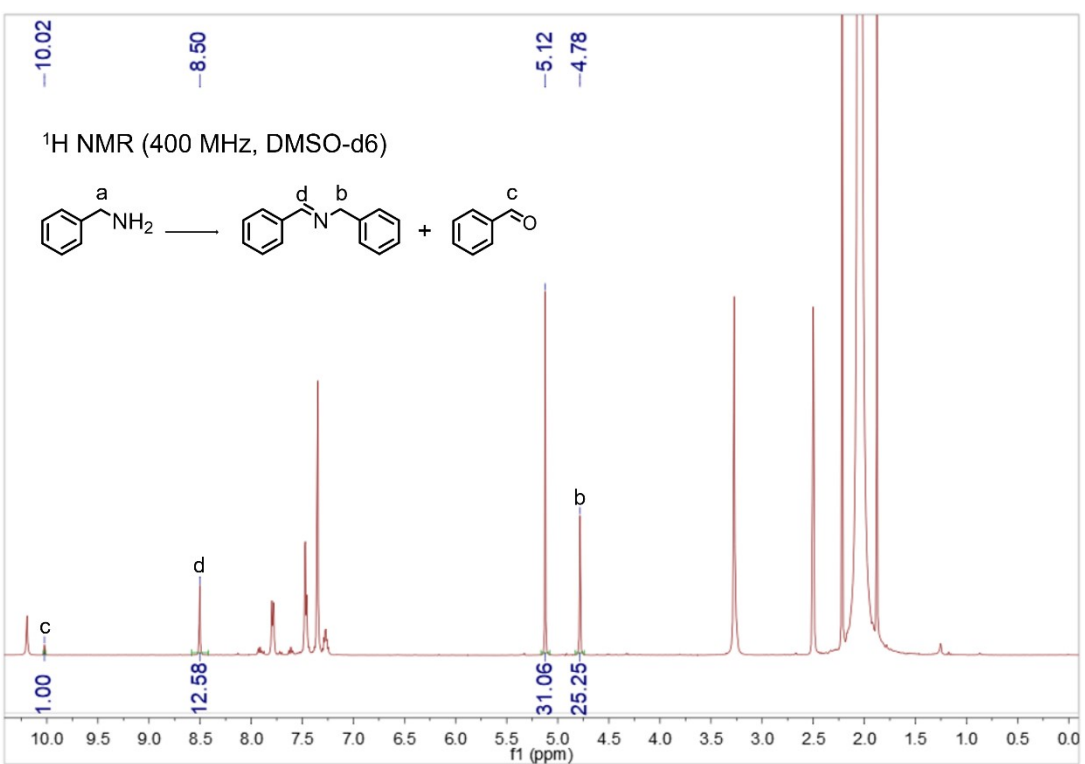
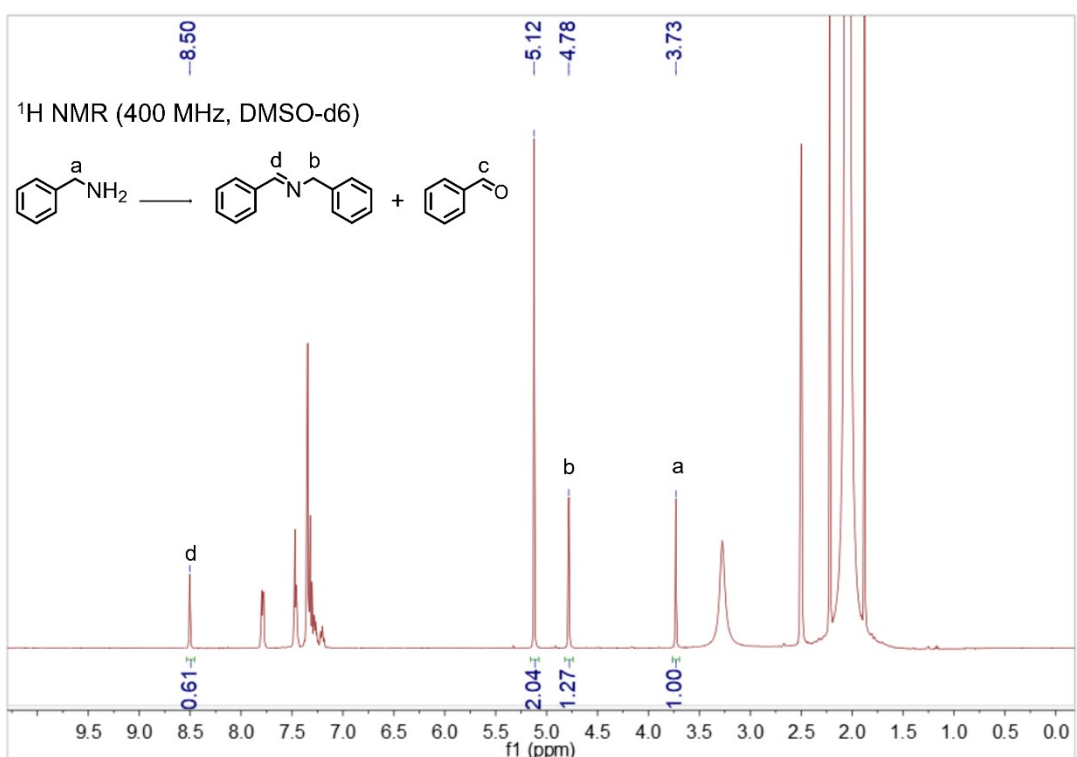


Fig. S7. ¹H NMR spectrum for photo-oxidative coupling of benzylamine catalyzed by o-PFC-1 at 1 h. The characteristic peak of 1,3,5-trioxane (internal standard) is at 5.12 ppm in DMSO-d6.

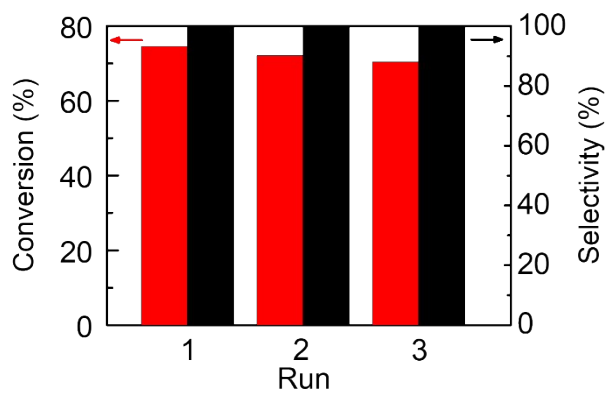


Fig. S8. Recycle performance of *p*-PFC-1 at 0.5 h using the oxidation of benzylamine as model reaction.

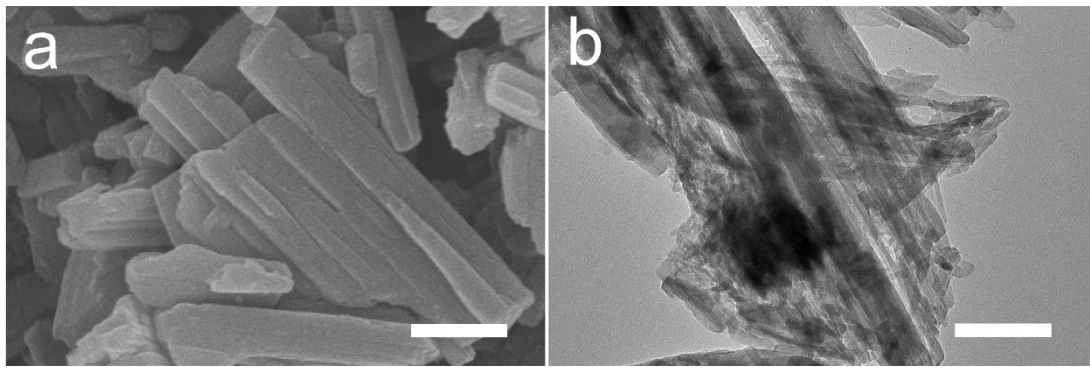
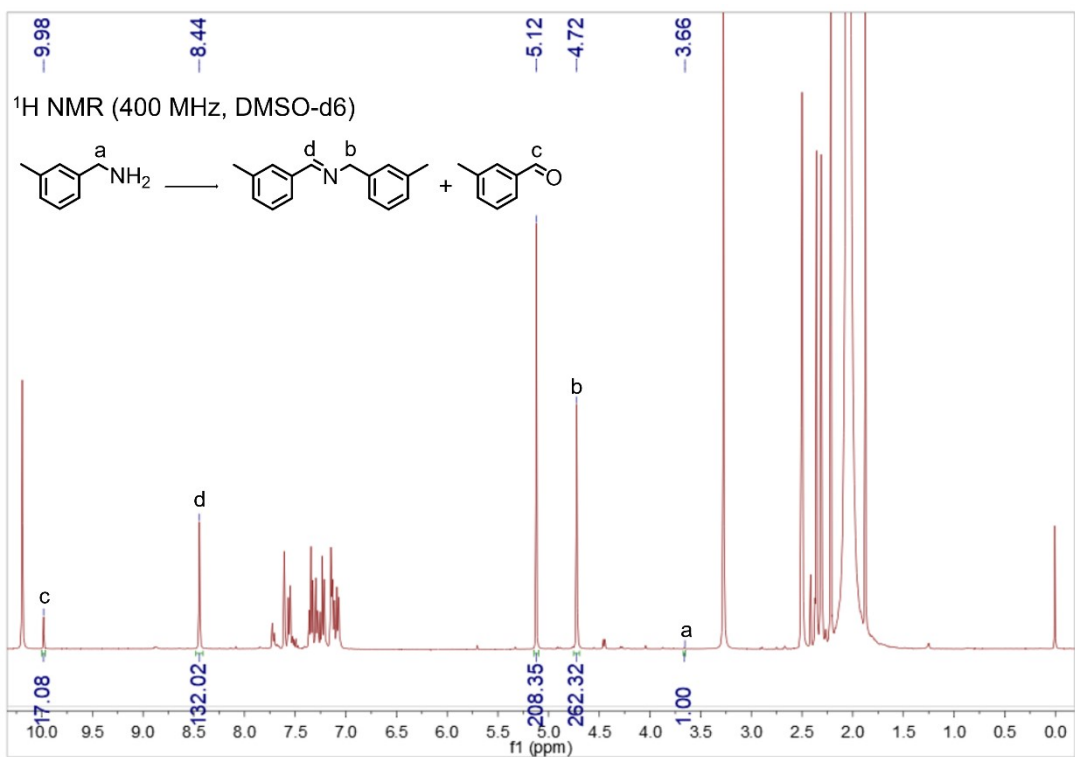
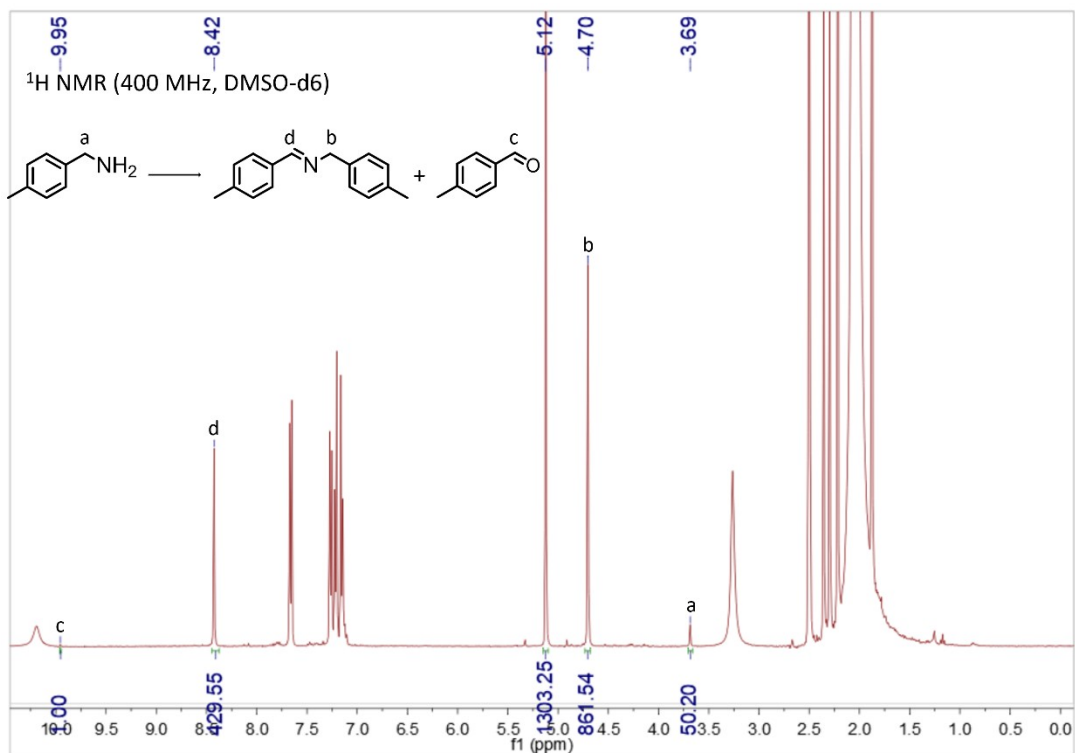
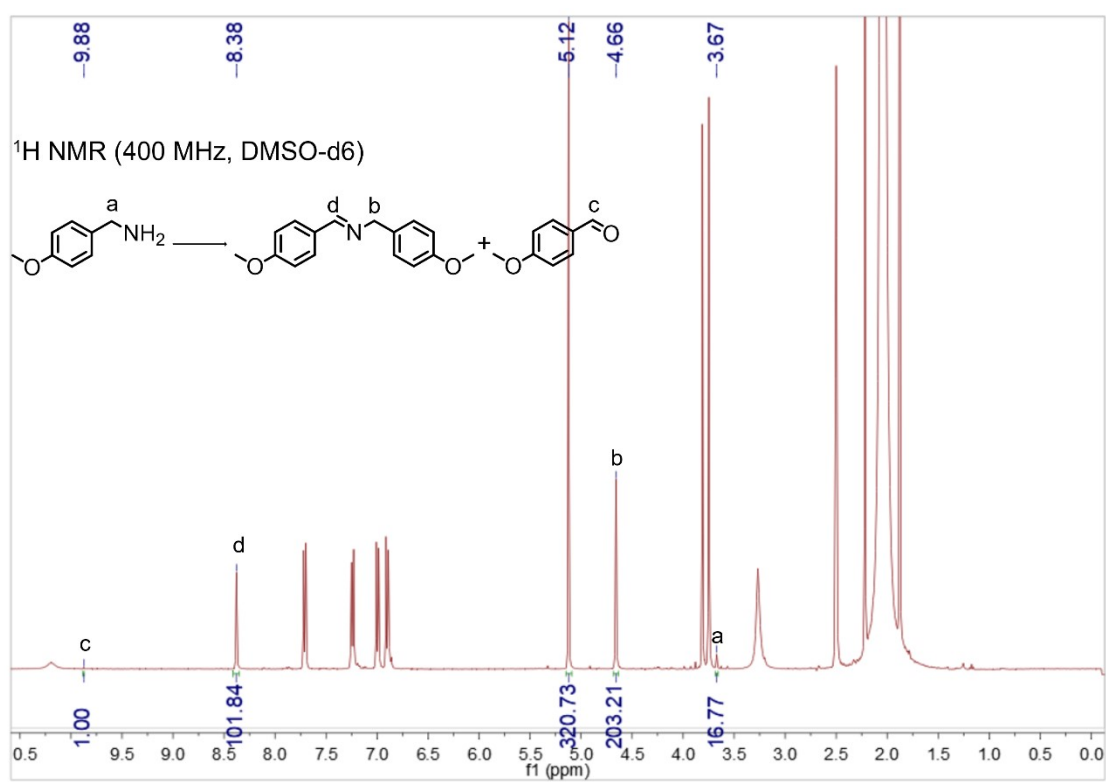
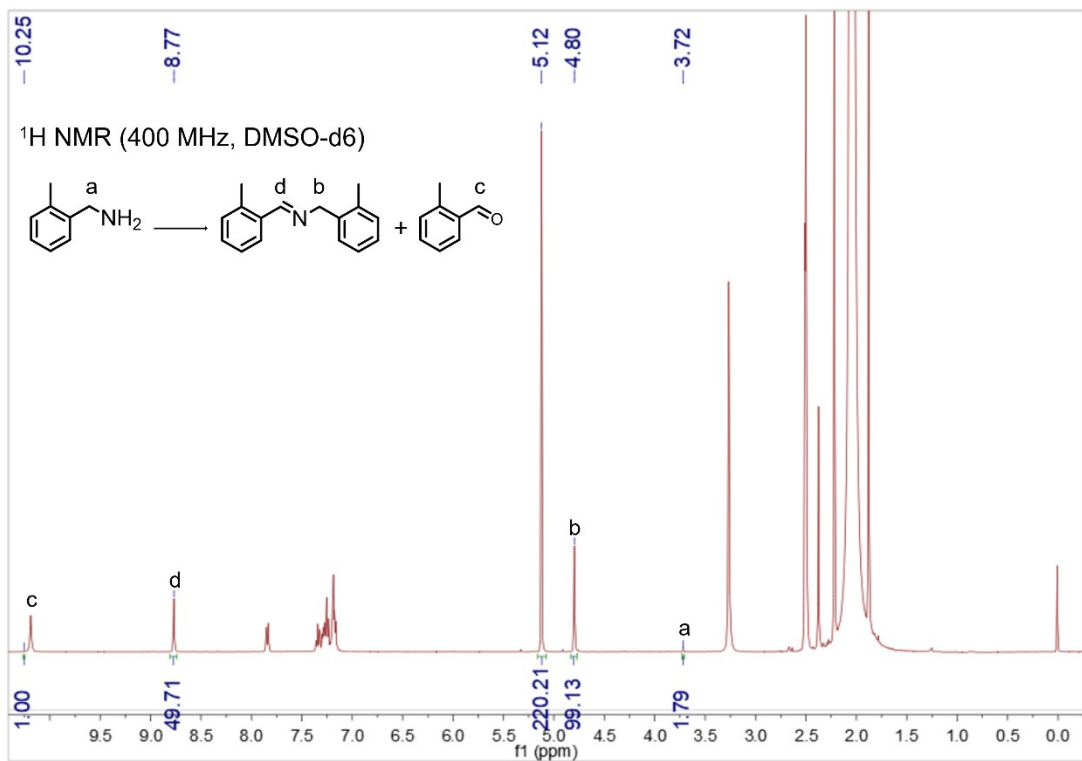
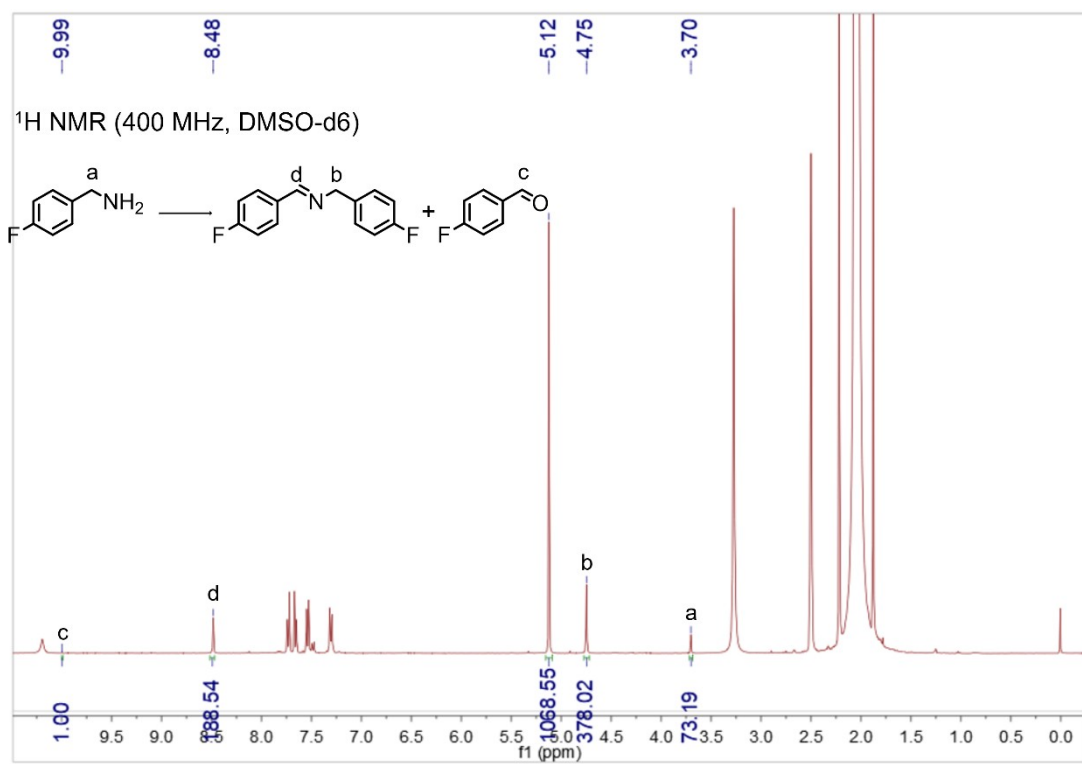
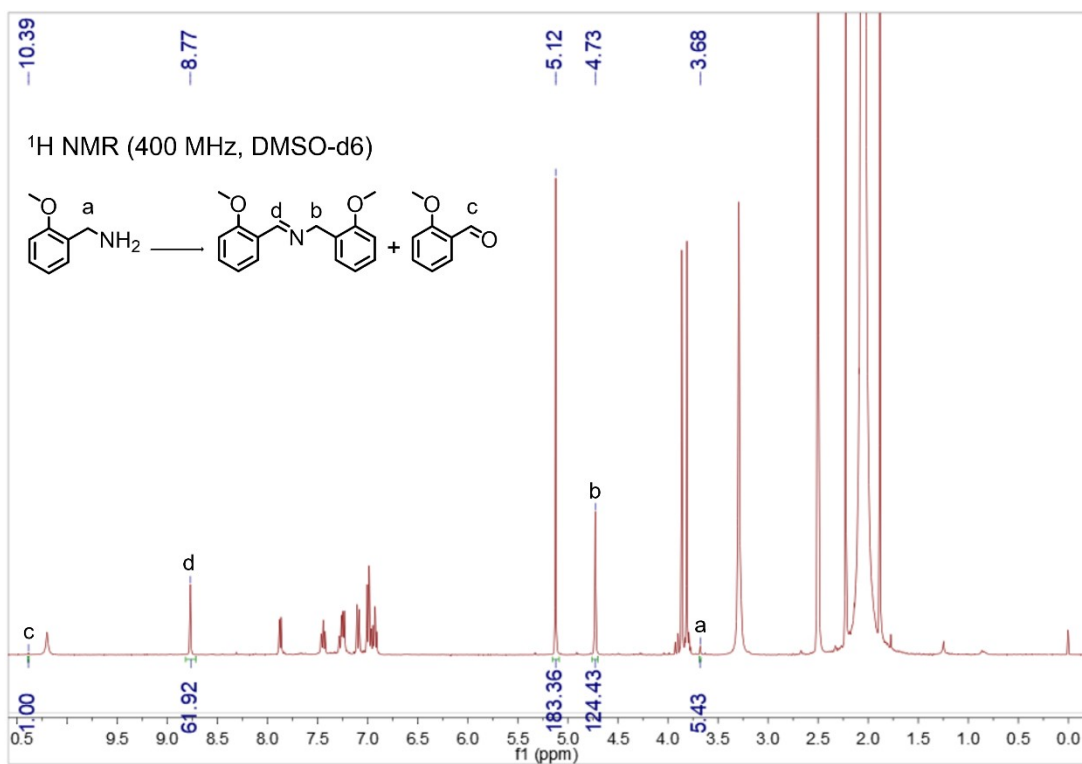
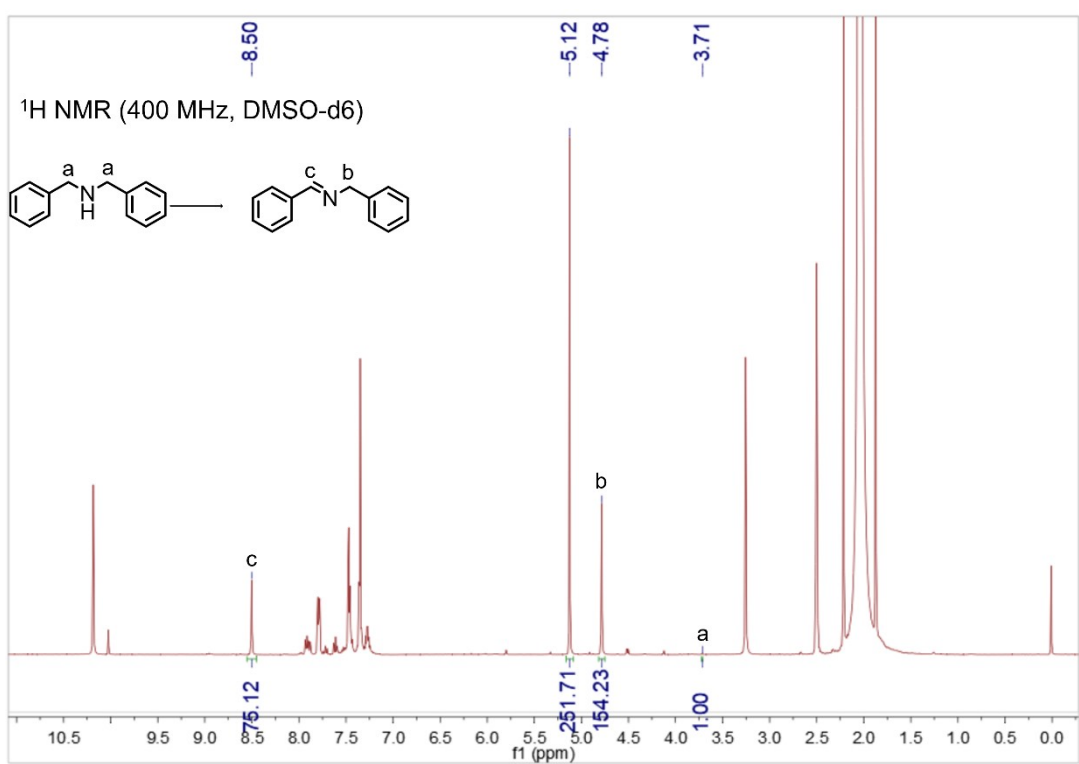
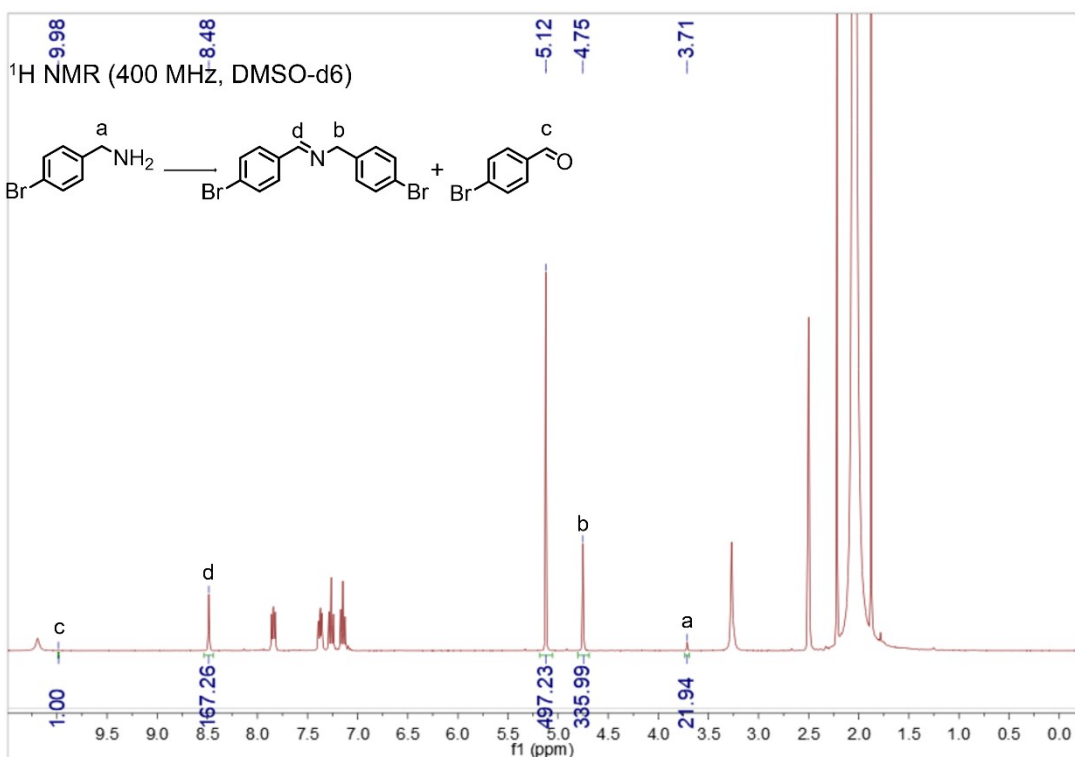


Fig. S9. SEM (a) and TEM (b) images of *p*-PFC-1 after 3 catalysis runs. Scale bars: 400 nm in (a) and 150 nm in (b).









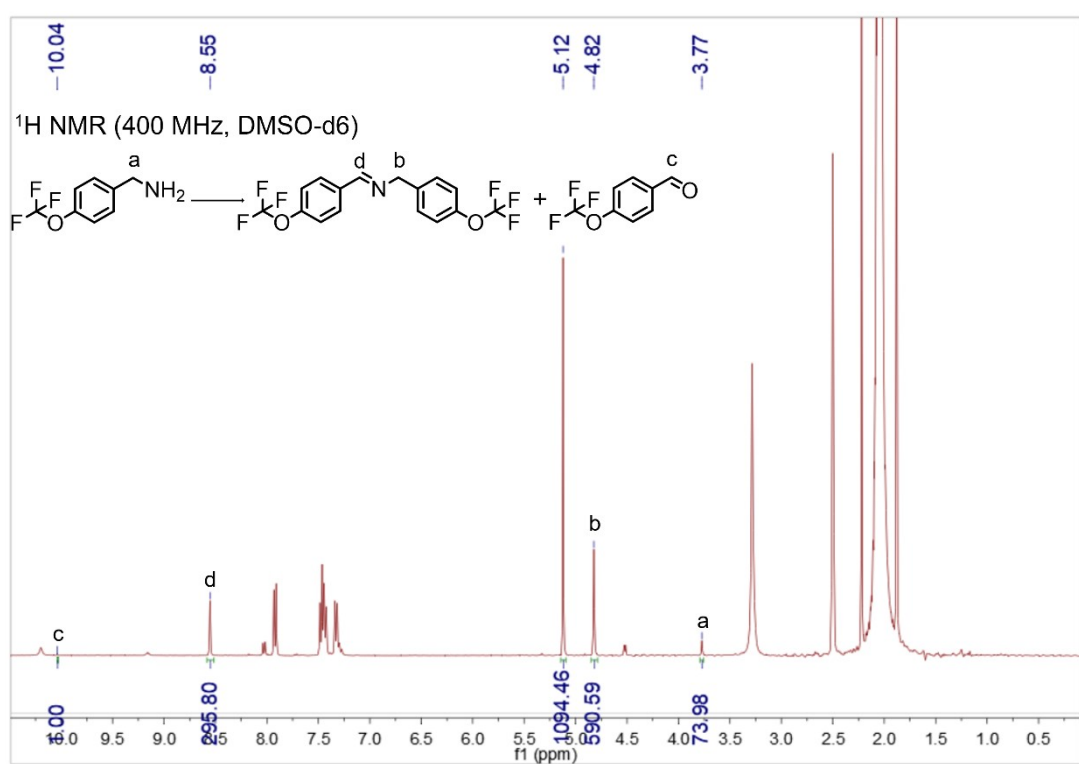
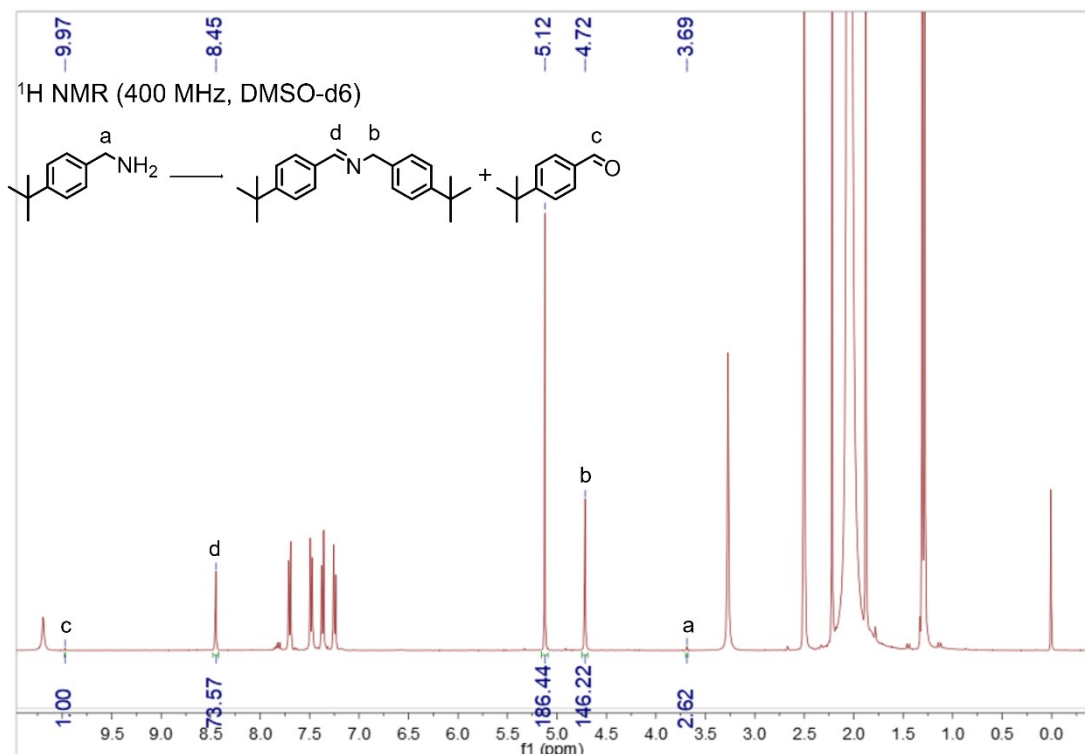


Fig. S10. ^1H NMR spectra for photo-oxidative coupling reactions of various benzylamine derivatives catalyzed by *p*-PFC-1 at 1 h. The characteristic peak of 1,3,5-trioxane (internal standard) is at 5.12 ppm in DMSO-d6.

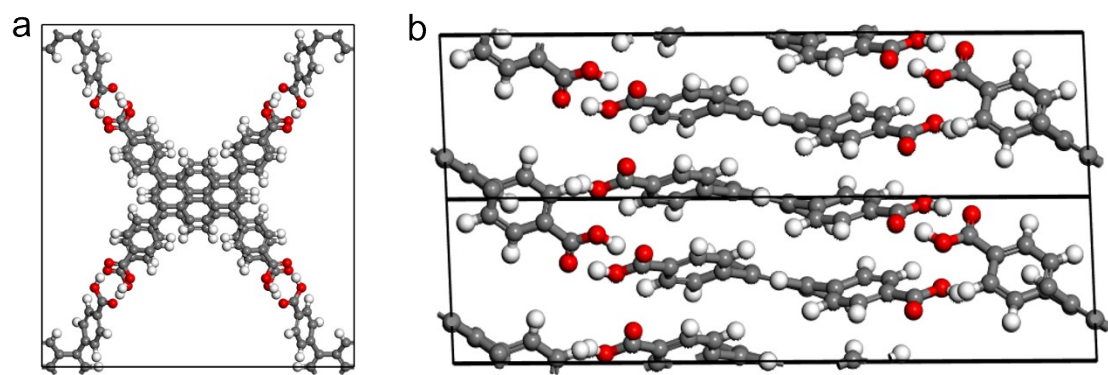


Fig. S11. Vertical (a) and side (b) views of theoretical models of *p*-PFC-1 used in DFT calculations.

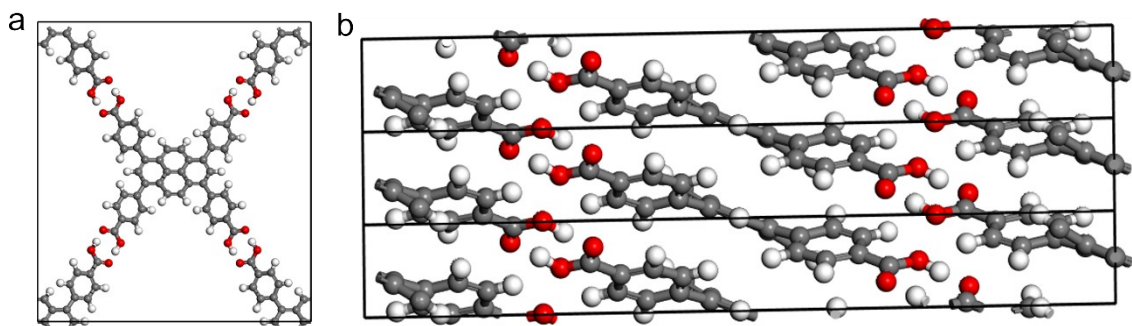
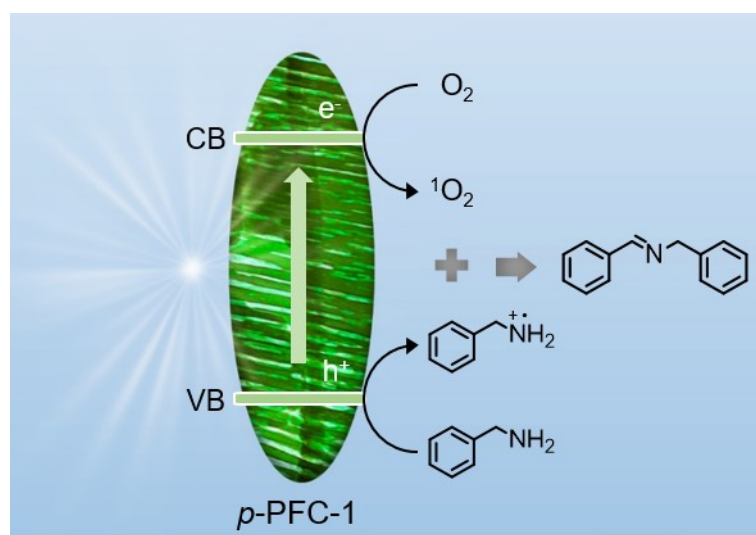


Fig. S12. Vertical (a) and side (b) views of theoretical models of *o*-PFC-1 used in DFT calculations.



Scheme S1. Reaction mechanism for photo-oxidative coupling of benzylamine catalyzed by *p*-PFC-1.

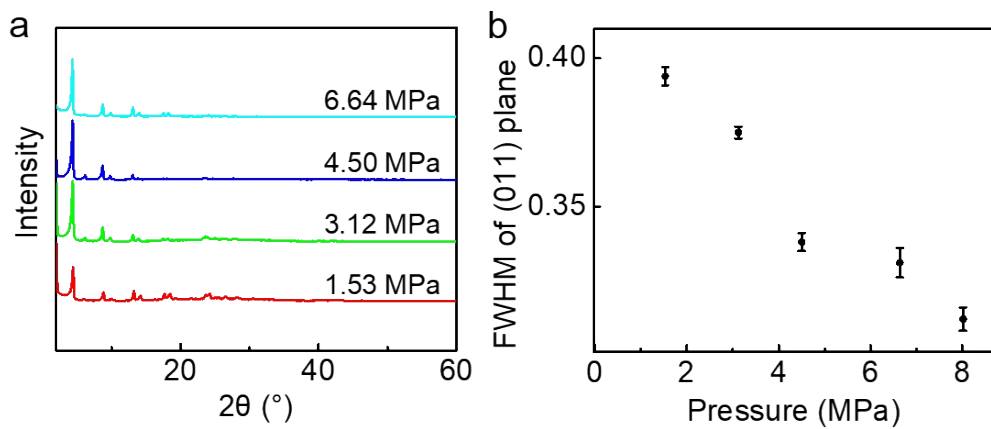


Fig. S13. (a) XRD patterns of PFC-1 synthesized at different pressures. (b) Dependence of the full-width half maximum (FWHM) values of (011) plane on pressure.

The main peaks in XRD patterns of PFC-1 obtained at pressure of 1.53, 3.12, 4.50 and 6.64 MPa match well with those of the simulated XRD of PFC-1, indicating the formation of PFC-1 in presence of compressed CO₂. Apparently, the FWHM value of (011) peak decreases for the PFC-1 sample synthesized at higher pressure. It means that high pressure CO₂ is favorable for accelerating the crystallization of PFC-1.

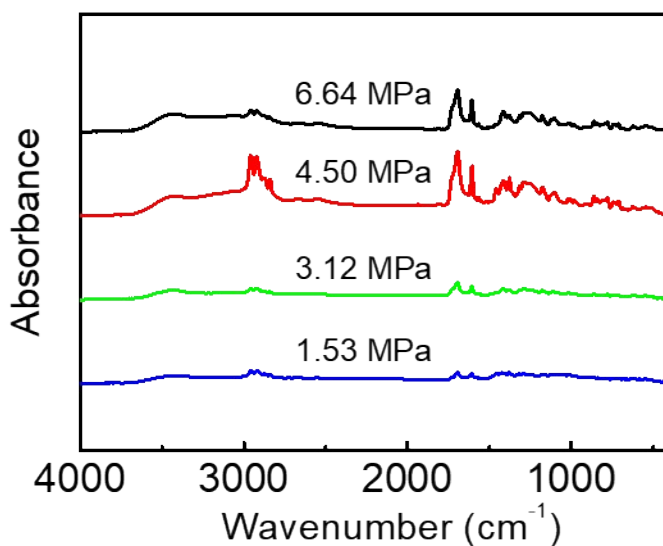


Fig. S14. FT-IR spectra of PFC-1 synthesized at 1.53, 3.12, 4.50 and 6.64 MPa, respectively.

FT-IR spectra of PFC-1 samples synthesized at 1.53, 3.12, 4.50 and 6.64 MPa show the characteristic bending vibration of $-\text{OH}$ (δ) at 1379, 1379, 1377 and 1379 cm^{-1} , respectively. Simultaneously, the four FT-IR spectra show that all the characteristic stretching vibration of C=O in carboxylic groups are at 1693 cm^{-1} . The two characteristic peaks of above materials are slightly shifted to lower wavenumber compared with those of H₄TBAPy (1383 and 1698 cm^{-1} , respectively). It can be assigned to the formation of hydrogen-bonds between C=O and $-\text{OH}$ in associated carboxylic groups of PFC-1, indicating the successful formation of PFC-1 synthesized at 1.53, 3.12, 4.50 and 6.64 MPa, respectively.

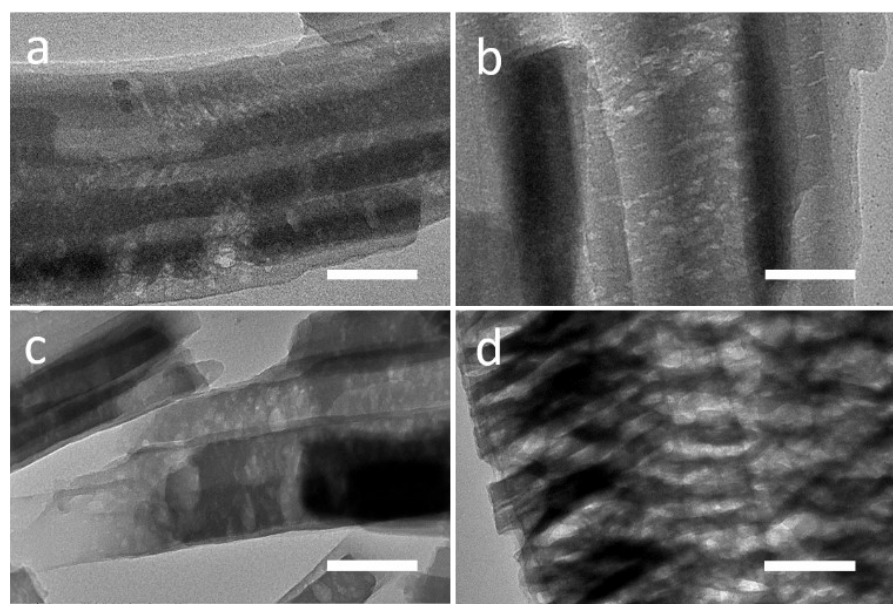


Fig. S15. TEM images of PFC-1 synthesized at 1.53 MPa (a), 3.12 MPa (b), 4.50 MPa (c) and 6.64 MPa (d). Scale bars: 100 nm.

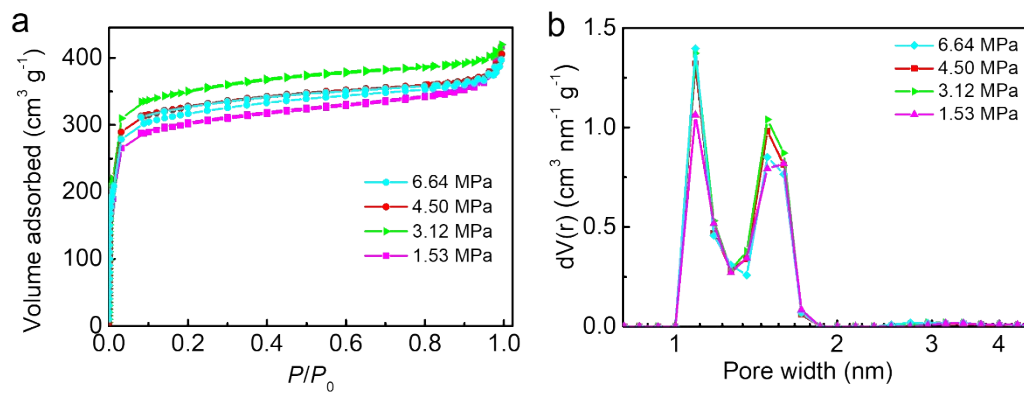


Fig. S16. (a) N₂ adsorption-desorption isotherms and (b) pore size distribution curves of PFC-1 synthesized at 1.53, 3.12, 4.50 and 6.64 MPa, respectively.

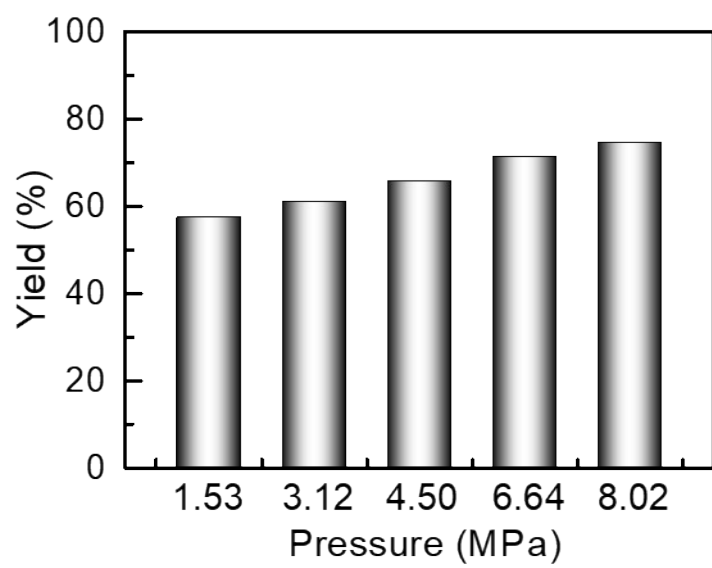


Fig. S17. Photocatalytic activities of benzylamine conversion of PFC-1 samples synthesized at 1.53, 3.12, 4.50, 6.64 and 8.02 MPa, respectively.

Table S1. Comparison of the reaction conditions and performances of different catalysts for photocatalytic oxidative coupling of benzylamine.

Catalysts	Conditions	Time (h)	Conv. ^[a] (%)	Select. ^[a] (%)	Production rate of <i>N</i> -benzylbenzaldimine (mmol g ⁻¹ h ⁻¹)	Ref.
<i>p</i> -PFC-1 (2 mg)	benzylamine (0.8 mmol), CH ₃ CN (5 mL), air, 25 °C, Xe lamp with a cutoff filter (380 < λ < 780 nm).	1	100	99.7	467.2	This work
Few-layer C ₃ N ₄ (15 mg)	benzylamine (0.5 mmol); 5 mL CH ₃ CN (5 mL); 0.1 MPa O ₂ , visible light (λ > 420 nm), 25 °C.	1	99	99	16.3187	3
SC-HM (semicrystalline heptazine-based melon polymer) (5 mg)	benzylamine (0.5 mmol), CH ₃ CN (2 mL), O ₂ (1 atm), Xe lamp (50 W) without filter, 20 °C.	4	99	99	12.2513	4
R-WO ₃ (defect-rich WO ₃) nanosheets (20 mg)	benzylamine (0.1 mmol), CH ₃ CN (4 mL), O ₂ (1 atm), light (λ > 400 nm, 100 mW cm ⁻²), rt.	8	~82	99	0.2539	5
TH550-3 (2D-TiO ₂) (10.0 mg)	benzylamine (0.2 mmol), CH ₃ CN (10.0 mL), O ₂ (0.1 MPa), UV-Vis light (20 mW cm ⁻²), 25 °C.	10	100	86.7	0.8670	6
R-PI	benzylamine (0.1 mmol), CH ₃ CN	6	90.5	98.5	0.1486	7

(conjugated polyimide) (50 mg)	(5 mL), 1 atm O ₂ , 80 °C, white LED (0.3 W cm ⁻²).					
NNU-45 (In-MOF) (4 mg)	benzylamine (0.2 mmol), O ₂ , DMSO (1 mL).	2.67	99	99	9.1884	8
Bi ₂₄ O ₃₁ Br ₁₀ (20 mg)	benzylamine (0.2 mmol), water (1 mL), O ₂ (1 atm), blue light.	12	98	97	0.3961	9
Au/M-TiO ₂ (20 mg)	benzylamine (0.2 mmol), CH ₃ CN (5 mL), O ₂ (1 atm), visible-light irradiation ($\lambda > 420$ nm).	8	96	99	0.5940	10
Tx-CMP (a metalfree truxene-based conjugated microporous polymer) (10 mg)	benzylamine (0.5 mmol), CH ₃ CN (5 mL), O ₂ atmosphere in direct sunlight.	4	>99	91	5.6306	11
CF-HCP (carbazole-fluorenone based porous hypercrosslinked polymer) (5.0 mg)	benzylamine (0.2 mmol), CH ₃ CN (2.0 mL), visible light, green LED lamp (520 nm, 30 W), O ₂ (1 atm).	6	91.0 ^[b]	-	3.0333	12
mixed phase 2D-MoS ₂ (28 wt%, 3 mg)	benzylamine (0.1 mmol), CH ₃ CN (3 mL), O ₂ balloon, 45 W white LED, 80 °C.	72	99	-	0.2292	13
MoS ₂ /rGO	benzylamine (0.5 mmol), <i>n</i> -	20	91	97	2.2068	14

composites (5 mg)	octane (2.5 mL), 120 °C, O ₂ (1 atm).					
m-O= C ₃ N ₄ (carbonyl- modified carbon nitride) (10 mg)	benzylamine (0.1 mmol), CH ₃ CN (5 mL), O ₂ balloon (0.1 MPa), light source: λ= 420 nm, rt.	4	>99	>99	1.2251	15
Agl-1000 (50 mg)	benzylamine (0.5 mmol), CH ₃ CN (10 mL), O ₂ (1 atm), 40 °C, light intensity (0.48 W cm ⁻² , 500 W Halogen lamp).	24	95	96	0.1900	16
ATA-BiOCl (2- aminoterephth halic acid (ATA) sensitized BiOCl nanosheet) (100 mg, 0.18 %)	benzylamine (0.1 mmol), CH ₃ CN (5 mL), 15 W fluorescent lamp (400 < λ < 800 nm), air (1 atm), 25 °C	24	100	100	0.0208	17
ZnIn ₂ S ₄ (8 mg)	benzylamine (0.1 mmol), CH ₂ Cl ₂ (2.0 mL), air.	0.75	99.0	94.0	7.7550	18
Zn-bpydc (10 mg)	benzylamine (0.5 mmol), DMF (5 mL), 300 W Xe lamp (350 < λ < 780 nm), air, 25 °C.	4	99.7	>99	6.2310	19
n-NH ₂ -MIL- 125	benzylamine (0.2 mmol), CH ₃ CN (4 mL), 300 W Xe lamp (350 < λ	9	98.5	99.0	1.0630	20

(10 mg)	< 780 nm), air, 25 °C.					
Cd(dcbpy) (10 mg)	benzylamine (0.48 mmol), DMF (5 mL), 300 W Xe lamp ($350 < \lambda$ < 780 nm), air, 25 °C.	7	99.1	>99	3.3980	21
PCN-222 (Zr-MOF) (5 mg)	benzylamine (0.1 mmol), 100 mW cm ⁻² Xe lamp ($\lambda \geq 420$ nm), CH ₃ CN (3 mL), air.	1	100	100	10	22
BiOBr-S-110 (100 mg)	benzylamine (0.1 mmol), CH ₃ CN (5 mL), 15 W Philips lamp (400 < λ < 650 nm), 25 °C, air.	14	100	100	0.0357	23
TiO ₂ (Degussa P25) (10 mg)	benzylamine (0.1 mmol), 100 W Hg lamp ($\lambda \geq 300$ nm), CH ₃ CN (5 mL), air (1 atm).	9	99	85	0.4675	24
OBBC/ms-BiVO ₄ binuclear complexes (200 mg)	benzylamine (500 uM, 0.1 mmol) solution, (200 mL, tetrahydrofuran (THF): CH ₃ CN = 98:2 v/v) with Cu(hfacac) ₂ (4.0 mm), ($\lambda > 430$ nm, 6 mW cm ⁻²), 25 °C under aerated conditions.	2	66.4	> 99	0.0830	25
COF (TFPT-BMTH) (5 mmol%, 5.6 mg)	benzylamine (0.2 mmol), H ₂ O (5 mL), rt, air, blue LED (30 W, $\lambda =$ 454 nm).	24	99	-	0.7366	26
BiOBr-OV (10 mg)	benzylamine (0.2 mmol), CH ₃ CN (1 mL), air, 20 °C, Xe lamp with a cutoff filter ($\lambda \geq 420$ nm).	12	96	99	0.7920	27
c-BiOCl	benzylamine (0.092 mmol), DMF	1	100	100	9.2	28

(10 mg)	(5 mL), air, 25 °C, 300 W Xe lamp (350 < λ < 780 nm).						
---------	--	--	--	--	--	--	--

^[a] Conversion (Conv.) and selectivity (Select.) were determined by ¹H NMR.

^[b] The yield of photocatalytic oxidative coupling of benzylamine.

Table S2. Effect of scavenger on benzylamine oxidative coupling catalyzed by *p*-PFC-1.^[a]

Entry	Scavenger	Quenching group	Conv. (%) ^[b]	Select. (%) ^[b]
1	beta-carotene	$^1\text{O}_2$	28.6	99.7
2	benzoquinone	$\text{O}_2^{\cdot-}$	90.2	99.7

^[a]Reaction conditions: 2 mg catalyst, 5 mL CH₃CN, 0.8 mmol benzylamine, 2 equivalent of scavenger, 1 h, 300 W Xe lamp (380 < λ < 780 nm). ^[b] Conversion (Conv.) and selectivity (Select.) were determined by ¹H NMR.

The conversion of benzylamine at 1 h drops from 100% to 28.6% in the presence of beta-carotene, which suggests that $^1\text{O}_2$ exists in the reaction system and serves as an reactive oxygen species (ROS) for the photocatalytic oxidative coupling of benzylamine. With benzoquinone (BQ) as a scavenger to capture $\text{O}_2^{\cdot-}$, the conversion of benzylamine at 1 h decreases to 90.2%. Obviously, beta-carotene can significantly suppress benzylamine oxidative coupling and BQ has slightly suppressed benzylamine oxidative coupling for *p*-PFC-1. The results indicate that $^1\text{O}_2$ is the major ROS for the photo-oxidative coupling reaction of benzylamine for *p*-PFC-1.

References

1. Y. Yano, N. Mitoma, K. Matsushima, F. J. Wang, K. Matsui, A. takakur, Y. Miyauchi, H. Ito and K. Itami, *Nature*, 2019, **571**, 387-392.
2. Q. Yang, Y. D. Chen, X. G. Duan, S. K. Zhou, Y. Niu, H. Q. Sun, L. J. Zhi and S. B. Wang, *Appl. Catal., B*, 2020, **276**, 119146.
3. Y. T. Xiao, G. H. Tian, W. Li, Y. Xie, B. J. Jiang, C. G. Tian, D. Y. Zhao and H. G. Fu, *J. Am. Chem. Soc.*, 2019, **141**, 2508-2515.
4. H. Wang, X. S. Sun, D. D. Li, X. D. Zhang, S. C. Chen, W. Shao, Y. P. Tian and Y. Xie, *J. Am. Chem. Soc.*, 2017, **139**, 2468-2473.
5. N. Zhang, X. Y. Li, H. C. Ye, S. M. Chen, H. X. Ju, D. B. Liu, Y. Lin, W. Ye, C. M. Wang, Q. Xu, J. F. Zhu, L. Song, J. Jiang and Y. J. Xiong, *J. Am. Chem. Soc.*, 2016, **138**, 8928-8935.
6. Q. F. Chen, H. Wang, C. C. Wang, R. F. Guan, R. Duan, Y. F. Fang and X. Hu, *Appl. Catal., B*, 2020, **262**, 118258.
7. P. Kong, H. Tan, T. Y. Lei, J. Wang, W. J. Yan, R. Y. Wang, E. R. Waclawik, Z. F. Zheng and Z. Li, *Appl. Catal., B*, 2020, **272**, 118964.
8. H. X. Wei, Z. F. Guo, X. Liang, P. Q. Chen, H. Liu and H. Z. Xing, *ACS Appl. Mater. Interfaces*, 2019, **11**, 3016-3023.
9. W. Zhao, C. X. Yang, X. Zhang, Y. Deng, C. Q. Han, Z. Y. Ma, L. Wang and L. Q. Ye, *ChemSusChem*, 2020, **13**, 116-120.
10. J. L. Yang and C.-Y. Mou, *Appl. Catal., B*, 2018, **231**, 283-291.
11. V. R. Battula, H. Singh, S. Kumar, I. Bala, S. K. Pal and K. Kailasam, *ACS Catal.*, 2018, **8**, 6751-6759.
12. Y. F. Zhi, K. Li, H. Xia, M. Xue, Y. Mu and X. M. Liu, *J. Mater. Chem. A*, 2017, **5**, 8697-8704.
13. Y. R. Girish, R. Biswas and M. De, *Chem. Eur. J.*, 2018, **24**, 13871-13878.
14. M. M. Wang, H. H. Wu, C. R. Shen, S. P. Luo, D. Wang, L. He, C. G. Xia and G. L. Zhu, *ChemCatChem*, 2019, **11**, 1935-1942.
15. J.-J. Zhang, J.-M. Ge, H.-H. Wang, X. Wei, X.-H. Li and J.-S. Chen,

- ChemCatChem*, 2016, **8**, 3441-3445.
16. Z. Zheng, C. Chen, A. Bo, F. S. Zavahir, E. R. Waclawik, J. Zhao, D. Yang and H. Zhu, *ChemCatChem*, 2014, **6**, 1210-1214.
17. A. J. Han, J. L. Sun, H. W. Zhang, G. K. Chuah and S. Jaenicke, *ChemCatChem*, 2019, **11**, 6425-6430.
18. L. Ye and Z. H. Li, *ChemCatChem*, 2014, **6**, 2540-2543.
19. Y. F. Sha, J. L. Zhang, D. X. Tan, F. Y. Zhang, X. Y. Cheng, X. N. Tan, B. X. Zhang, B. X. Han, L. R. Zheng and J. L. Zhang, *Chem. Commun.*, 2020, **56**, 10754-10757.
20. X. N. Tan, J. L. Zhang, J. B. Shi, X. Y. Cheng, D. X. Tan, B. X. Zhang, L. F. Liu, F. Y. Zhang, B. X. Han and L. R. Zheng, *Sustainable Energy Fuels*, 2020, **4**, 2823-2830.
21. J. B. Shi, J. L. Zhang, T. L. Liang, D. X. Tan, X. N. Tan, Q. Wan, X. Y. Cheng, B. X. Zhang, B. X. Han, L. F. Liu, F. Y. Zhang and G. Chen, *ACS Appl. Mater. Interfaces*, 2019, **11**, 30953-30958.
22. C. Y. Xu, H. Liu, D. D. Li, J.-H. Su and H.-L. Jiang, *Chem. Sci.*, 2018, **9**, 3152-3158.
23. A. J. Han, H. W. Zhang, G.-K. Chuah and S. Jaenicke, *Appl. Catal., B*, 2017, **219**, 269-275.
24. X. J. Lang, H. W. Ji, C. C. Chen, W. H. Ma and J. C. Zhao, *Angew. Chem., Int. Ed.*, 2011, **50**, 3934-3937.
25. S. I. Naya, T. Niwa, R. Negishi, H. Kobayashi and H. Tada, *Angew. Chem., Int. Ed.*, 2014, **126**, 14114-14117.
26. Z. Q. Liu, Q. Su, P. Y. Ju, X. D. Li, G. H. Li, Q. L. Wu and B. Yang, *Chem. Commun.*, 2020, **56**, 766-769.
27. H. Wang, D. Y. Yong, S. C. Chen, S. L. Jiang, X. D. Zhang, W. Shao, Q. Zhang, W. S. Yan, B. C. Pan and Y. Xie, *J. Am. Chem. Soc.*, 2018, **140**, 1760-1766.
28. B. X. Zhang, J. L. Zhang, R. Duan, Q. Wan, X. N. Tan, Z. Z. Su, B. X. Han, L. R. Zheng and G. Mo, *Nano Energy*, 2020, **78**, 105340.